BAECC: a field campaign to elucidate the impact of Biogenic Aerosols on Clouds and Climate

Petäjä, T., O'Connor, E. J., Moisseev, D., Sinclair, V. A., Manninen, A. J., Väänänen, R., von Lerber, A., Thornton, J. A., Nicoll, K., Petersen, W., Chandrasekar, V., Smith, J. N., Winkler, P. M., Kruger, O., Hakola, H., Timonen, H., Brus, D., Laurila, T., Asmi, E., Riekkola, M.-L., Mona, L., Massoli, P., Engelmann, R., Komppula, M., Wang, J., Kuang, C., Bäck, J., Virtanen, A., Levula, J., Ritsche, M. T. and Hickmon, N. (2016)
BAECC: a field campaign to elucidate the impact of Biogenic Aerosols on Clouds and Climate. Bulletin of the American Meteorological Society, 97 (10). pp. 1909-1928. ISSN 1520-0477 doi: https://doi.org/10.1175/BAMS-D-14-00199.1
Available at https://centaur.reading.ac.uk/65660/

BAECC
A FIELD CAMPAIGN TO ELUCIDATE THE IMPACT OF BIOGENIC AEROSOLS ON CLOUDS AND CLIMATE

BY TUUKKA PETÄJÄ, EWAN J. O'CONNOR, DMITRI MOISSEEV, VICTORIA A. SINCLAIR, ANTTI J. MANNINEN, RIIKKA VÄÄNÄNEN, ANNAKAISA VON LERBER, JOEL A. THORNTON, KERI NICOLL, WALT PETERSEN, V. CHANDRASEKAR, JAMES N. SMITH, PAUL M. WINKLER, OLAF KRÜGER, HANNELE HAKOLA, HILKKA TIMONEN, DAVID BRUS, TUOMAS LAURILA, EIJA ASMI, MARJA-LIISA RIEKKOLA, LUCIA MONA, PAOLA MASSOLI, RONNY ENGELMANN, MIKA KOMPPULA, JIAN WANG, CHONGAI KUANG, JAANA BÄCK, ANNELE VIRTANEN, JANNE LEVULA, MICHAEL RITSCHE, AND NICKI HICKMON

Observations obtained during an 8-month deployment of AMF2 in a boreal environment in Hyytiälä, Finland, and comprehensive in situ data from the SMEAR II station enable the characterization of biogenic aerosol, clouds, and precipitation and their interactions.

The boreal forest atmosphere provides an ideal locale to study aerosol and cloud microphysical processes. In this clean environment, the contribution of biogenic emissions and subsequent increases in secondary aerosol number (e.g., Kulmala et al. 2007, 2013) and mass (e.g., Tunved et al. 2006) enables assessment of the importance of natural aerosol in the aerosol–cloud interactions. Anthropogenic influences and signatures in aerosol particle size distributions (PSDs) are evident even at the cleanest sites (Carslaw et al. 2013). However, with a suitably long time series, analyses of aerosol–cloud interactions in such an environment can be used for assessing the role of both natural and anthropogenic emissions in global climate, especially over boreal and Arctic regions, which are experiencing drastic changes because of the ongoing climate change (Epstein et al. 2013; Koenigk et al. 2013).

The largest uncertainty in climate predictions comes from aerosol–cloud interactions (Boucher et al. 2013). A lack of comprehensive observations of cloud and precipitation systems in different climatic regimes is one of the key reasons for this uncertainty (Stephens and Kummerow 2007). Because of the complexity of different feedback mechanisms linking global climate with aerosols, trace gases, and precipitation, regional and global climate models are unable to reliably predict precipitation patterns and their changes (Rosenfeld et al. 2008; Ren et al. 2013). As a result, climatologically meaningful connections between aerosols, clouds, and precipitation have not yet been established (Stevens and Feingold 2009). An approach postulated to address this problem is the "deployment of arrays of ground-based remote sensors that can both vertically and temporally resolve the aerosol, clouds, precipitation and the meteorological state" and to document cloud and precipitation processes in different regimes (Stevens and Feingold 2009, p. 611). This holistic approach capturing the life cycles of aerosols, clouds, and precipitation was adopted for the campaign Biogenic Aerosols–Effects on Clouds and Climate (BAECC; Petäjä 2013).

During BAECC, the U.S. Department of Energy (DOE)'s Atmospheric Radiation Measurement (ARM) Program deployed their Second ARM Mobile Facility (AMF2) in Hyytiälä, Finland (61°51′N, 24°17′E), for an 8-month intensive measurement campaign from February to September 2014 (Fig. 1). Hyytiälä hosts the Station for Measuring Ecosystem–Atmosphere Relations II (SMEAR II; Hari and Kulmala 2005; see sidebar on "Hyytiälä: History and significant scientific advances"). The primary research goal of BAECC is to understand how biogenic aerosols affect cloud microphysical properties.

OBSERVATIONS. To reach the holistic research goals, a comprehensive measurement approach is required. During BAECC this was provided through the complementary strengths of SMEAR II and AMF2 capabilities. SMEAR II ecophysiological measurements and in situ observations of the physical, chemical, and optical properties of aerosol particles and ions were complemented with the ground-based active remote sensing capacity of the AMF2 radar and lidar systems. Additional supplementary observations on aerosol chemical composition, aerosol precursors, nanoparticle concentrations, precipitation properties, and aerosol and water vapor vertical profiling were provided by collaborators from the United States and Europe, both for the whole observation period and during intensive observation periods (IOPs; Fig. 1). During IOPs, a total of 152 flight hours with Cessna and Skyvan aircraft provided in situ data on trace gases, aerosol particle concentration, and aerosol chemical composition. Traditional meteorological soundings (4 day^{-1}) were enhanced with novel miniaturized solar radiation, charge, and turbulence sensors during two of the IOPs. In addition to the AMF2 radars, precipitation and cloud properties above Hyytiälä were provided by the Finnish Meteorological Institute (FMI) operational dual-polarization weather radar once every 15 min. One IOP was dedicated to documenting snowfall microphysics through a combination of multifrequency (C, X, Ka, and W band) radar, microwave radiometer (MWR), and lidar measurements supplemented by a comprehensive suite of surface-based precipitation observations. For a comprehensive list of observations, see Table SB1.

Both SMEAR II and the AMF2 Aerosol Observation System (Jefferson 2011) performed in situ measurements of aerosols during BAECC, including cloud condensation nuclei (CCN) concentrations and optical properties. Datasets collected by both facilities have been compared for quality assurance and control. Moreover, additional in situ measurements deployed in the same area allow for the assessment of small-scale spatial variability in aerosol concentration and size distribution.

On the regional scale, the representativeness of the datasets will be evaluated by the continuous and coordinated aerosol observations performed at five other SMEAR aerosol observation network sites in Finland and by the four aircraft IOPs. The existing 20-yr-long measurement data from SMEAR II enables

AFFILIATIONS: Petäjä, Sinclair, Manninen, Väänänen, and Krüger—Department of Physics, University of Helsinki, Helsinki, Finland; O'Connor—Finnish Meteorological Institute, Helsinki, Finland, and Department of Meteorology, University of Reading, Reading, United Kingdom; Moisseev—Department of Physics, University of Helsinki, and Finnish Meteorological Institute, Helsinki, Finland; von Lerber, Hakola, Timonen, Brus, Laurila, and Asmi—Finnish Meteorological Institute, Helsinki, Finland; Thornton—University of Washington, Seattle, Washington; Nicoll—Department of Meteorology, University of Reading, Reading, United Kingdom; Petersen—Wallops Flight Facility, National Aeronautics and Space Administration Goddard Space Flight Center, Wallops Island, Virginia; Chandrasekar—Department of Physics, University of Helsinki, and Finnish Meteorological Institute, Helsinki, Finland, and Colorado State University, Fort Collins, Colorado; Smith—National Center for Atmospheric Research, Boulder, Colorado, and Department of Applied Physics, University of Eastern Finland, Finland, and University of California, Irvine, Irvine, California; Winkler—Faculty of Physics, University of Vienna, Vienna, Austria; Riekkola—Department of Analytical Chemistry, University of Helsinki, Helsinki, Finland; Mona—Istituto di Metodologie per l'Analisi Ambientale, Consiglio Nazionale delle Ricerche Tito Scalo, Potenza, Italy; Massoli—Institute of Atmospheric Sciences and Climate (ISAC), Bologna, Italy, and Aerodyne Research Inc., Billerica, Massachusetts; Engelmann—Leibniz Institute for Tropospheric Research, Leipzig, Germany; Komppula—Finnish Meteorological Institute, Kuopio, Finland; Wang and Kuang—Brookhaven National Laboratory, Upton, New York; Bäck—Department of Forest Sciences, University of Helsinki, Helsinki, Finland; Virtanen—Department of Applied Physics, University of Eastern Finland, Finland; Levula—Department of Physics, University of Helsinki, Helsinki, Finland, and Station for Measuring Ecosystem–Atmosphere Relations II, Hyytiälä, Finland; Ritsche and Hickmon—Argonne National Laboratory, Lemont, Illinois

CORRESPONDING AUTHOR: Tuukka Petäjä, Department of Physics, University of Helsinki, Gustaf Hällströmin katu 2, 00014 Helsinki, Finland
E-mail: tuukka.petaja@helsinki.fi

The abstract for this article can be found in this issue, following the table of contents.
DOI:10.1175/BAMS-D-14-00199.1

In final form 8 January 2016

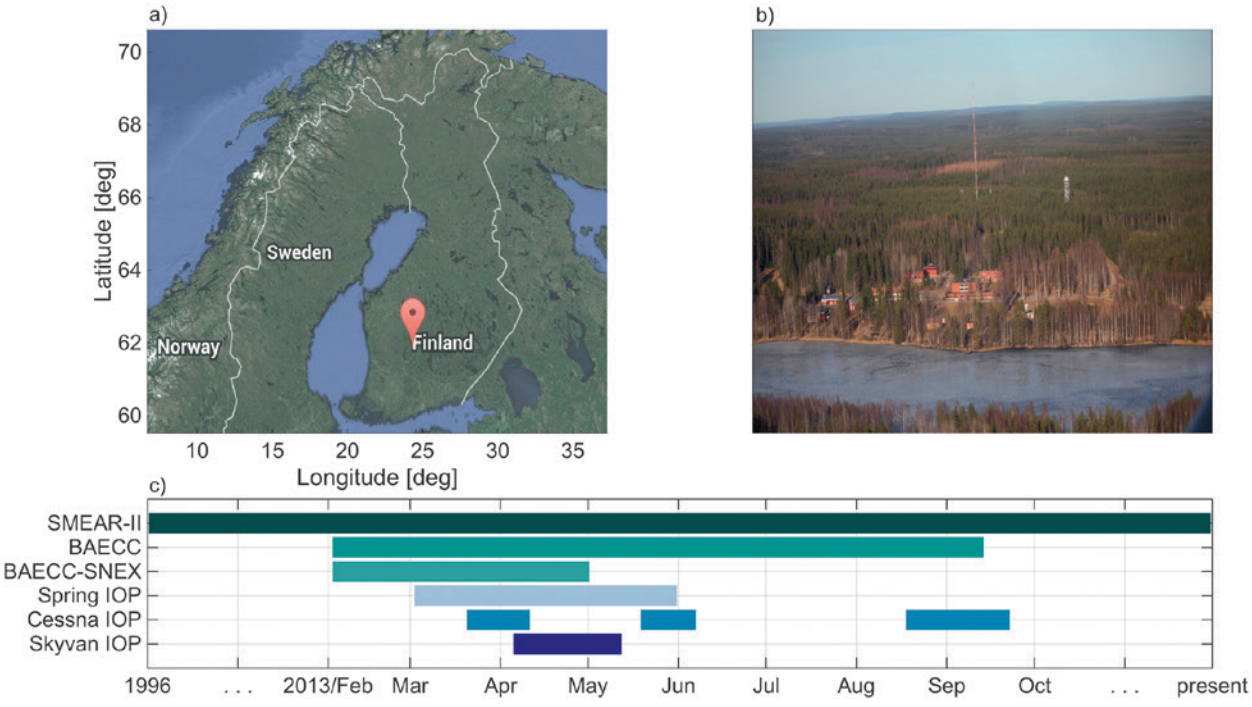

Fig. 1. (a) The BAECC campaign was performed in Hyytiälä. (b) AMF2 was collocated with SMEAR II with (c) several specific IOPs organized during the deployment. SMEAR II has been providing data for the last two decades.

the assessment of the representativeness of the data collected during the BAECC period. The utilization of the SMEAR observation network, Aerosols, Clouds, and Trace Gases Research Infrastructure Network (ACTRIS), and Global Atmospheric Watch data provides avenues for expanding the analysis to an even larger extent. The data from SMEAR II are available via Junninen et al. (2009) and from smartSMEAR (2016). AMF2 data are available from the ARM data archive (ARM 2015).

EMISSIONS TO AEROSOLS. Of all biomes, the boreal forests appear to have the largest biogeophysical effect on the annual-mean global temperature (Bonan 2008). The forest is a net sink for carbon dioxide consumed in vegetation photosynthesis. Furthermore, the boreal environment is a substantial source of biogenic volatile organic compounds (BVOCs), which can affect tropospheric ozone (Atkinson and Arey 2003), and BVOCs are associated with frequent secondary aerosol formation (e.g., Kulmala et al. 2001; Dal Maso et al. 2005; Tunved et al. 2006; Kulmala et al. 2013).

The emissions of BVOCs in the boreal forest arise through evaporation from specialized storage structures (Guenther et al. 1995) and from de novo biosynthesis (Ghirardo et al. 2010). Environmental factors, such as temperature and the amount of photosynthetic active radiation, govern the emissions, but environmental stress factors, such as drought and ozone exposure, may increase or decrease emissions. There is also considerable variation between individual trees in their BVOC emission fingerprints, which, in Scots pine, are composed of a variable mixture of alpha-pinene, beta-pinene, delta-carene, and sesquiterpenes (e.g., Hakola et al. 2006; Bäck et al. 2012). Additionally, new needle development and growth processes can be large sources of BVOCs (e.g., Aalto et al. 2015) associated with spring recovery of the ecosystem (Dal Maso et al. 2009). Approximately 80% of BVOC emissions in a conifer forest stand originate from trees, with the rest from the soil (Aaltonen et al. 2011), and both source strengths were measured with automated cuvettes during the BAECC campaign (Table 1).

The winter temperatures during the BAECC period were abnormally mild, with photosynthesis (net carbon uptake) persisting even in February, leading to increased emissions of BVOCs. This indicated that the potential for biogenic production of precursor gases was high during the spring months. Monoterpenes are the main emitted compound group from coniferous forests around Hyytiälä (Hakola et al. 2006). The shoot-scale enclosure measurements with proton transfer mass spectrometry revealed that, as in many previous years, extremely high emission rates in early spring coincided with the spring recovery period of trees during early–mid-March and that these peaks

Table 1. AMF2 and SMEAR2 measurements and time lines of the IOPs during BAECC.

Continuous measurements	
AMF2 (Data available from ARM data archive: www.archive.arm.gov/armlogin/login.jsp; ARM 2015)	**SMEAR II (Selected data available from SmartSMEAR portal: www.atm.helsinki.fi/smartSMEAR; Junninen et al. 2009)**
Aerosol optical properties (nephelometer)	Aerosol number size distribution [1 nm–10 μm, particle size magnifier (PSM), differential mobility particle sizer (DMPS), neutral cluster and air ion spectrometer (NAIS), and aerodynamic particle sizer (APS)]
Aerosol number concentration > 10 nm [condensation particle counter (CPC)]	Aerosol number concentration (PSM, CPC)
Atmospheric profiling (radiosoundings)	Atmospheric ion distribution [AIS, balanced scanning mobility analyzer (BSMA)]
Thermodynamic state of the atmosphere	Aerosol optical properties (scattering, absorption, and extinction)
Wind speed and direction	Total and size resolved cloud condensation nuclei counter (CCNC)
Boundary layer height (ceilometer)	Aerosol vertical profile, boundary layer height, wind, and cloud-base height (HALO Photonics doppler lidar, Vaisala ceilometer)
Cloud-base height [ceilometer, micro pulse lidar (MPL)]	Aerosol volatility distribution [volatility differential mobility particle sizer (VDMPS); Häkkinen et al. 2012]
CCNC	Aerosol mass concentration (impactor sampling, on-line mass analyzer)
Cloud particle size distribution [X-band scanning ARM cloud radar (XSACR)]	Aerosol chemical composition [aerosol chemical speciation monitor (ACSM), Sunset EC/OC analyzer, monitor for aerosols and gases in ambient air (MARGA), filter sampling for off-line analysis]
Hydrometeor fall velocity (XSACR)	Trace gas concentrations and profiles (NO, NO_x, O_3, SO_2, H_2O, CO_2, CO, COS, and VOC)
Hygroscopic growth [hygroscopic tandem differential mobility analyzer (HTDMA)]	Ecosystem-scale fluxes: latent, sensible heat, CO_2, CH_4, COS, CH_4, and aerosols
Liquid water path (LWP)	Biosphere–atmosphere exchange (VOC, CO_2, H_2O, NO_x, and O_3) from branch, soil, and tree stems
Ozone concentration	Chlorophyll fluorescence of pine needles
Profiles of aerosol backscatter, extinction and depolarization [high spectral resolution lidar (HSRL)]	Sap flow, stem properties, needle, and stem growth
Radar Doppler [marine W-band ARM cloud radar (MWACR), Ka-band zenith pointing radar (KAZR)]	Surface meteorology and profiles 2–127 m
Radar polarization (XSACR)	Solar radiation (global, ultraviolet A and B, photosynthetically active radiation, spectroradiometer, reflected, direct and diffuse, and up and down)
Radar reflectivity (XSACR, MWACR, KAZR)	Longwave radiation radiation (up/down)
Surface meteorology (ARM surface meteorological system)	Radon, radioactivity
Vertical velocity (KAZR)	

provide 2–3 times higher monoterpene emissions compared to the rest of spring (Aalto et al. 2015). The maximum emission rates were observed during 11–12 March 2014, with another high-emission period seen during new foliage growth in late May–early June (Aalto et al. 2014). During summer, the highest emissions coincided with high temperatures in early and late summer, whereas the relatively cool weeks around midsummer resulted in lower monoterpene emissions.

The emissions from the biosphere together with their oxidation products lead to new particle formation (Kulmala et al. 2004, 2013). This process provides a major source of particles in clean boreal forests (Fig. 2; Kulmala et al. 2001). Although many precursors (sulfuric acid, amines, and various organic vapors) have been attributed to initial gas-to-particle conversion, the dominant process growing these clusters to climatically relevant sizes is, without doubt, condensation of organic vapors (Kulmala et al. 1998; Riipinen et al. 2011; Zhou et al. 2014). This fact is also underlined by the typical chemical composition observed, which indicates that the majority of particulate mass in natural boreal forests is made up of organic compounds (Jimenez et al. 2009).

Aerosol formation occurred frequently during BAECC (Fig. 2). The concentration of nanoparticles was probed with a suite of scanning particle size magnifiers (PSM; Vanhanen et al. 2011) and the mobile versatile size-analyzing nuclei counter (vSANC; Pinterich et al. 2016) in the size range 1–5 nm at ground level and at 35-m height. Overall, the seasonal cycle of events during BAECC was typical for Hyytiälä with a maximum in spring and a secondary maximum in autumn. The separation of ion-induced and neutral pathways was determined

Table 1. Continued.

IOP measurements	
Spring IOP: Initial steps of aerosol formation and subsequent growth	**Airborne IOP: Skyvan (FMI)**
Dates: Mar–May 2014	Dates: Sep 2014
Atmospheric ion chemical composition; atmospheric pressure interface–time of flight mass spectrometer (APiTOF; Junninen et al. 2010)	Distribution of aerosols, clouds and precipitation [cloud, aerosol, and precipitation probe (CAPS)]
Peroxy- and organic peroxy radicals (HO_x, RO_x CI-APiTOF; R. L. Mauldin et al. 2015, unpublished manuscript)	Aerosol particle and cloud hydrometeor size distributions (0.51–50 μm)
Stabilized Criegee intermediate concentration and lifetime (Taipale et al. 2014)	Temperature and pressure
Atmospheric ion concentrations and vertical profiles (BSMA, Sigma)	Liquid water content (0.01–3 g m^{-3})
Sulfuric acid, extremely low volatility organic compounds (ELVOC), clusters (nitrate chemical ionization (CI) APiTOF; Jokinen et al. 2012);	Particle optical properties (refractive index)
Organic acids (acetate CI-APiTOF)	Particle shape assessments
Ion mobility and composition [ion mobility spectrometer IMS)-APiTOF]	Precipitation size distributions
Precursors, aerosol composition, fluxes [filter inlet for gases and aerosols (FIGAERO) with chemical ionization mass spectrometer (CIMS); Lopez-Hilfiker et al. 2014]	Aerosol properties via BMI isokinetic inlet
Aerosol chemistry [thermal desorption chemical ionization mass spectrometer (TDCIMS; Smith et al. 2008); high resolution time of flight aerosol mass spectrometer (HR-AMS; DeCarlo et al. 2006)]	Chemical composition [Aerodyne high resolution soot particle aerosol mass spectrometer (HR SP AMS)]
VOC characterization and profiles [proton transfer reaction time of flight mass spectrometer (PTRTOFMS) and PTR quadrupole mass spectrometer (PTRQMS)]	Optical extinction (Aerodyne CAPS-PMx instrument)
Atmospheric cluster concentrations, physical characterization (PSM, NAIS, vSANC; Pinterich et al. 2016)	Cloud condensation nuclei concentrations (Droplet Measurement Technologies, CCNc 100)
Aerosol-phase state and hygroscopicity [aerosol bounce instrument (ABI; Virtanen et al. 2011; HTDMA)	Aerosol particle number concentration 10 nm–3 μm (TSI CPC 3010)
	Black carbon concentration (DMT SP2, MicroAeth AE51)
	Trace gases (Picarro)
	Airborne IOP: Cessna (UHEL)
	Dates: 24 Mar–11 Apr, 19 May–07 Jun, and 18 Aug–19 Sep 2014
	Carbon dioxide and water vapor concentration (LI-840)
	Aerosol particle number concentration [3 nn–3 μm; ultrafine CPC (UCPC)]
	Aerosol number size distribution [10–400 nm; scanning mobility particle sizer (SMPS)]
	Temperature, static air pressure, relative humidity
	Ion and naturally charged aerosol size distribution (1–44 nm; NAIS)

through measurements of both ions and neutral particle concentrations, with the neutral pathway dominating formation rates. Figure 2 displays an example of a new particle formation event starting from sub-3-nm sizes during the morning hours of 23 April. During subsequent days, as the synoptic situation remained unchanged, these particles grew larger in size, leading to a factor of 10 increase in the concentration of CCN-sized particles.

Typically, higher concentrations of precursor vapors enhance aerosol growth (Kulmala et al. 2001; Riipinen et al. 2012). There are indications that some of the organic molecules are also relevant for the initial steps of aerosol formation (Riccobono et al. 2014; Schobesberger et al. 2013a; Kirkby et al. 2016; Tröstl et al. 2016). During BAECC concentrations of condensable vapors, such as sulfuric acid (Petäjä et al. 2009) and extremely low volatile organic compounds (ELVOC; Ehn et al. 2014), were measured with a suite of mass spectrometers. To contrast observations with other available long-term data, proxy variables were developed to capture the temporal variability of the relevant vapor concentrations (Petäjä et al. 2009; Mikkonen et al. 2011). Atmospheric oxidation of the aerosol precursors was probed by measuring atmospheric oxidants, such as ozone, HO_x + RO_x (R. L. Mauldin et al. 2015, unpublished manuscript), and stabilized Criegee intermediates (Taipale et al. 2014) during the BAECC spring IOP (Table 1).

Based on a Filter Inlet for Gases and Aerosols chemical-ionization mass spectrometer (FIGAERO-CIMS

HYYTIÄLÄ: HISTORY AND SIGNIFICANT SCIENTIFIC ADVANCES

The history of the Hyytiälä forestry field station goes back over 100 years. The University of Helsinki founded the station to enable forestry teaching and research in field conditions in 1910. Atmospheric research has been part of Hyytiälä station since the mid-1980s as a result of an interdisciplinary Finnish Acidification Research Programme (HAPRO; Kauppi et al. 1990) and because of the Chernobyl nuclear power plant accident in April 1986 as Hyytiälä was in the area of the radioactive fallout (Raunemaa et al. 1987; Nygren et al. 1994). These events paved the road to establishing a continuous, comprehensive measurement station dedicated to forest–atmosphere interactions. In 1995, the operational phase of SMEAR II (Hari and Kulmala 2005) was started. After 20 years of measurements and incessant development, SMEAR II features the most comprehensive atmospheric observations with the longest continuous time series, for example, on submicron aerosol number size distributions.

One of the key findings of SMEAR II has been that secondary aerosol formation from gas-phase precursors is a frequent phenomenon in the boreal environment (Mäkelä et al. 1997; see Fig. 2 for an example from the BAECC campaign), occurring on average every fourth day. This process is most active during spring, when on almost half of the days we observe the appearance of sub-3-nm aerosol particles and their subsequent growth (Dal Maso et al. 2005). A secondary maximum of the events takes place in autumn. A typical source strength associated with the events is 1 cm^{-3} s^{-1} with growth rates varying from 0.5 to 8 nm h^{-1} (Kulmala et al. 2004). As this process takes place in a clean environment, this relatively small source, occurring over a large area, is able to produce particles large enough to activate as cloud droplets (Kerminen et al. 2012) and contribute up to 60% of the CCN-sized particles in the region (Merikanto et al. 2009).

Once the events were discovered, the quest to find the precursor vapors, their concentrations, and detailed mechanism commenced. The pathway is dominated by neutral nucleation, and the role of ions is limited (Kulmala et al. 2007). Laboratory experiments have identified several key vapors contributing to the initial steps of aerosol formation, such as sulfuric acid (Sipilä et al. 2010), ammonia (e.g. Kirkby et al. 2011), amines (Petäjä et al. 2011; Almeida et al. 2013), and organics (Riccobono et al. 2014; Tröstl et al. 2016). All of these compounds can enhance cluster stability and initial growth and therefore contribute to the process (Kulmala et al. 2013). In continental locations, such as Hyytiälä, sulfuric acid has been identified as a crucial ingredient (Weber et al. 1995; Petäjä et al. 2009), but its concentration is not high enough to explain further growth to climatically relevant particle sizes (Kulmala et al. 1998). In the boreal environment, the role of organic vapors in the growth is important (Riipinen et al. 2012), supported by the dominance of organics in the bulk chemical composition (Jimenez et al. 2009). A very plausible candidate for the vapor responsible for the aerosol growth to CCN sizes is a group of compounds called ELVOCs that readily participates both in the early stages of clustering and the growth (Ehn et al. 2014).

The modern high-resolution mass spectrometry (e.g., Ehn et al. 2010; Smith et al. 2010; Jokinen et al. 2012; Lopez-Hilfiker et al. 2014) together with the capacity to perform physical characterization of nanoparticles below 3 nm in size (Kulmala et al. 2007, 2013b) has led to breakthroughs in understanding the initial steps of aerosol formation in the boreal environment as well as in their subsequent growth to CCN sizes (Kerminen et al. 2012). The next stage of research requires the combination of measurements (in situ and active remote sensing) and multiscale modeling tools (quantum chemical modeling, process-level modeling, and regional and global models) to resolve the vertical and spatial variability of the processes affecting aerosol–cloud–climate interactions.

(Lopez-Hilfiker et al. 2014) and thermal desorption CIMS (TDCIMS; Smith et al. 2004) measurements, contributions to particulate mass were deduced from the partitioning of oxidation products from major biogenic VOC precursors such as monoterpenes, isoprene and/or methyl butene-1-ol, and either gas- or particle-phase accretion products of these species. Nitrogen-containing organics were also observed and may be a tracer of anthropogenic NO_x influence or may arise from nighttime chemistry involving the nitrate radical. Monoterpene concentrations were quite high (Fig. 2), and FIGAERO data show that monoterpene oxidation products dominated particulate mass during spring. TDCIMS data during spring showed that recently formed nucleation-mode particles contained higher fractions of oxidized hydrocarbons than older particles, supporting the link between highly oxidized gas-phase compounds and new particle formation. However, as spring progressed, FIGAERO observations showed a noticeable enhancement in the contribution of lower molecular weight compounds containing four to five carbon atoms, likely due to the onset of isoprene emissions with the leaf out of broad-leaved trees and increasing temperatures (Yassaa et al. 2012). Overall, a consistent composition appeared, with large contributions from monoterpene oxidation products, dimers, and nitrogen-containing organics, suggesting a role for anthropogenic influence even in this rural site. An important caveat to the last point is that natural soil emissions of NO_x or amines may constitute the dominant source of nitrogen-containing organics at this site. This aspect will be assessed as our analysis progresses.

Bulk aerosol chemical composition measurements in the submicron size range with aerosol

chemical composition were performed using an Aerosol Chemical Speciation Monitor (ACSM, Aerodyne Research Inc.; Ng et al. 2011). Data coverage during the BAECC campaign was extensive, with a good dataset obtained for studying the seasonality of the aerosol-phase composition. Increased organic contributions during the most photosynthetically active seasons was clearly observed, whereas in wintertime, anthropogenic sulfate reached its maximum, composing up to 25% of the nonrefractory submicron mass.

EXTENDING SURFACE MEASUREMENTS INTO THE VERTICAL. Based on direct observations inside clouds, Kerminen et al. (2005) showed that secondary aerosols formed from biogenic emissions can be activated to become cloud droplets. However, unraveling the mechanisms by which biogenic aerosol interacts with clouds requires that the vertical profile of aerosol, clouds, and turbulence be fully characterized in tandem. The process can be split into two main steps: the transport of biogenic aerosol from the surface into the boundary layer and free troposphere and the participation in cloud formation.

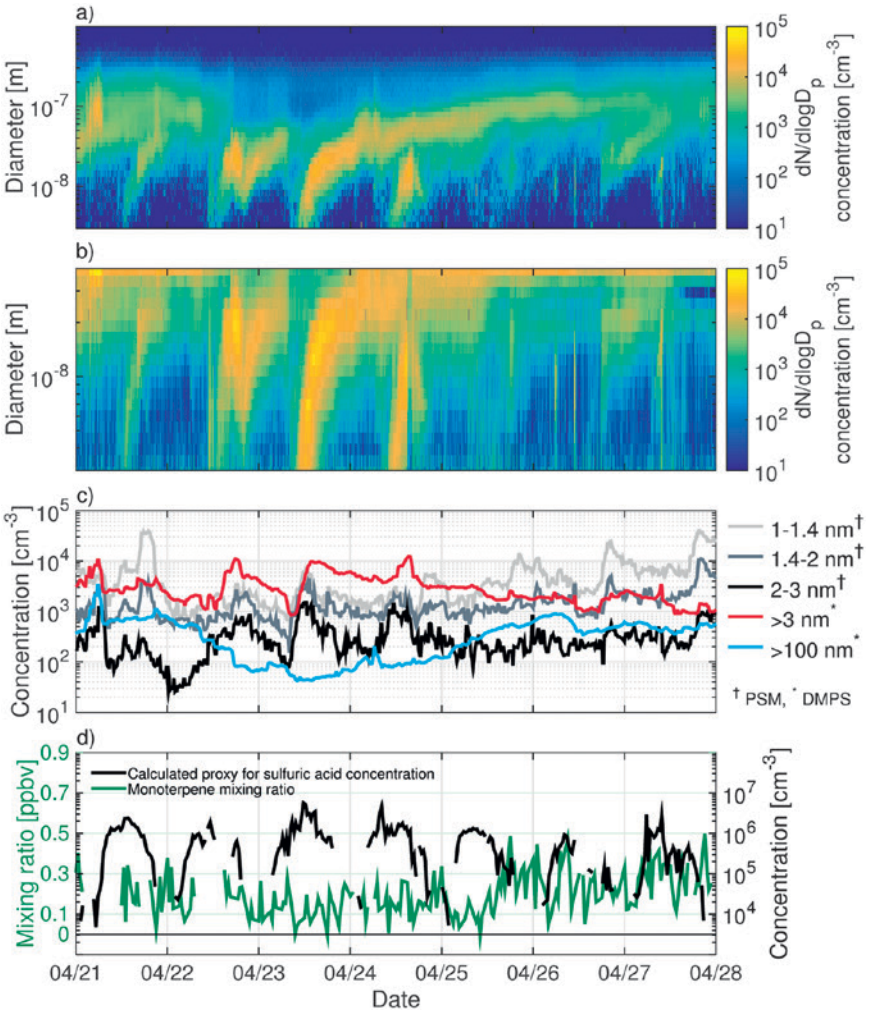

Fig. 2. An example of typical new particle formation events illustrated with PSD plots measured by (a) a differential mobility particle sizer (DMPS) and (b) a neutral cluster and air ion spectrometer (NAIS). (c) Time series of the smallest size-range aerosol particle concentrations measured with PSM together with the >3- and >100-nm particles measured with DMPS. (d) A time series of monoterpene mixing ratio with a proxy for sulfuric acid concentration at Hyytiälä during 21–27 Apr 2014.

The vertical profile of aerosol above the SMEAR II site was studied extensively through the use of remote sensing by lidar and by in situ aircraft-based measurements during three flight IOPs. Continuous remotely sensed vertical profiles of aerosol were obtained from a multitude of lidar instruments. These operated quasi continuously throughout the entire campaign period. For the instrumentation and timing of IOPs, the reader is referred to Table 1.

The transport of biogenic aerosol from the surface into the boundary layer is driven by turbulent mixing. This mixing ensures that all air within the turbulent layer is in intermittent contact with the surface, on time scales from 10 to 30 minutes, with the top of this layer termed the mixing-layer height (MLH; e.g., Emeis et al. 2008). The MLH can be defined in terms of the turbulent kinetic energy dissipation rate (Barlow et al. 2011), determined directly from the high-resolution vertically pointing (O'Connor et al. 2010) and scanning (Vakkari et al. 2015) Doppler lidar data provided by FMI at Hyytiälä. The potential for aerosol-layer identification and aerosol typing through a combination of backscatter coefficient and circular depolarization ratio is clearly shown in Figs. 3 and 4. Humid boundary layers, dry elevated layers, and humid elevated

layers can all be distinguished in high-spectral-resolution lidar (HSRL) data.

The flight IOPs took place in three seasons: early spring, beginning of summer, and beginning of autumn. The University of Helsinki (UHEL) operated a Cessna FR172F single-engine light aircraft modified to carry aerosol instrumentation as described in Schobesberger et al. (2013b). Figure 3 shows simultaneous measurements with Cessna and ARM HSRL on 2 April 2014. The flight path for this particular day is typical of the route selected during the flight campaigns. It is oriented in the south–north direction and consists of an initial ascent up to 3.5 km and then several legs at different altitudes above and within the boundary layer. In total, 144 flight hours were flown during 33 days with the Cessna, and all flights were in the vicinity of the SMEAR II station. During the flight IOP at the beginning of autumn, FMI operated a Short SC.7 Skyvan, an unpressurized aircraft (Short Brothers and Harland Ltd., Northern Ireland, United Kingdom) owned by Aalto University. Inclusion of chemical composition profiles from Skyvan flights (Fig. 4) permits the correct choice of refractive index when deriving microphysical properties from the lidar profiles. The details of the instrumentation in both aircraft are presented in Table 1.

The microphysical retrievals can be improved through harnessing data from the multiwavelength Raman lidar system Polly^{XT} (Althausen et al. 2009; Engelmann et al. 2016), where available, through collaboration with the European Aerosol Research Lidar Network (EARLINET; Pappalardo et al. 2014), now within ACTRIS. The combination of multiple channels through the use of the "3 backscatter + 2 extinction + 1 depolarization" approach allows aerosol typing (e.g., Mona et al. 2012; Mattis et al. 2004) and the retrieval of aerosol microphysical optical properties through the application of specific inversion algorithms (Müller et al. 1999; Veselovskii et al. 2005). The retrievals have been demonstrated to have the unique ability of providing range-resolved aerosol effective radius and a complex refractive index (e.g., Müller et al. 2007). The addition of sun photometer observations may permit the determination of the aerosol mass concentration profile, including separation of the fine and course components (Chaikovsky et al. 2016; Lopatin et al. 2013; Binietoglou et al. 2015). The range-resolved properties (e.g., aerosol size distribution, refractive index, single-scattering albedo, mass concentration, and water vapor) can then be independently verified at the surface and from the aircraft. The impact of humidity on aerosol depolarization ratios retrieved from lidar can also be examined in detail, with Fig. 4 showing how closely these two parameters can be linked (low depolarization values imply spherical hygroscopic aerosol, high depolarization values imply dry nonspherical aerosol).

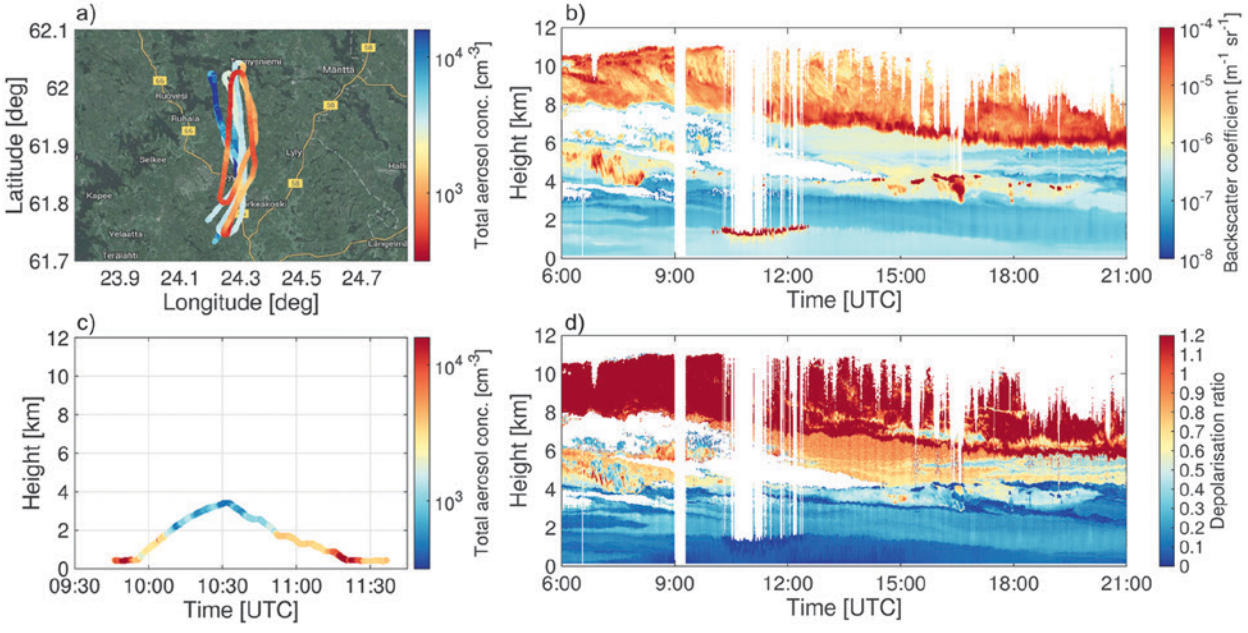

Fig. 3. UHEL Cessna (a) flight track and (c) altitude track during an aircraft IOP centered on Hyytiälä on 2 Apr 2014. The color of the track provides the total aerosol number concentration. (b) ARM backscatter coefficient and (d) circular depolarization ratio data for the same day, showing the potential for aerosol-layer identification and aerosol typing. Aircraft data from three IOPs (a total of 144 flight hours during 33 days with the UHEL Cessna) provide essential validation of remote sensing techniques.

Such a dataset will help identify the relative impact of long-range transport of material and local sources, and we will also investigate the mechanisms for dispersion. Besides confirming the remote sensing methods, the in situ data obtained by the aircraft can be used either as input or validating data for different atmospheric models, such as the model to simulate the concentrations of organic vapors, sulfuric acid, and aerosols (SOSAA; Boy et al. 2011). The inclusion of chemical composition (Fig. 4) and Picarro trace gas profiles from Skyvan provides a direct measurement of the impact of the environment on the aerosol properties during their transport from the surface into the boundary layer.

CLOUD VERTICAL PROFILING. Well-established ARM and Cloudnet (Illingworth et al. 2007) algorithms were used to derive vertical profiles of cloud properties for the entire campaign. The vertical profile of cloud macrophysical properties, including layer boundaries and phase, was obtained from a combination of vertically pointing Doppler cloud radar [Ka-band ARM zenith radar (KAZR) or marine W-band ARM cloud radar (MWACR) when KAZR is unavailable] and lidar (HSRL and ceilometer), following Illingworth et al. (2007). Combinations of various radar wavelengths (including scanning instruments operating at vertical) together with lidars and microwave radiometers were then used to retrieve the cloud microphysical properties, such as water content and flux, size distributions, and ice morphology. Drizzle properties, including median equivolumetric size, number concentration, drizzle liquid water content, and drizzle liquid water flux, were derived using a combination of KAZR (or MWACR) and a ceilometer (O'Connor et al. 2005).

Investigating the influence of biogenic aerosols on clouds requires that both the aerosol and cloud properties can be measured reliably and within the same volume. This poses a challenge since it is difficult to measure aerosol properties within the cloud by remote sensing methods. However, when considering liquid clouds coupled with the boundary layer, it is safe to assume that the vertical column within and below cloud is well mixed, producing well-defined profiles and gradients of atmospheric properties. In a well-mixed column, in-cloud properties can then be related to below-cloud aerosol properties and, in principle, to aerosol properties (such as size distribution, chemical composition, and hygroscopicity)

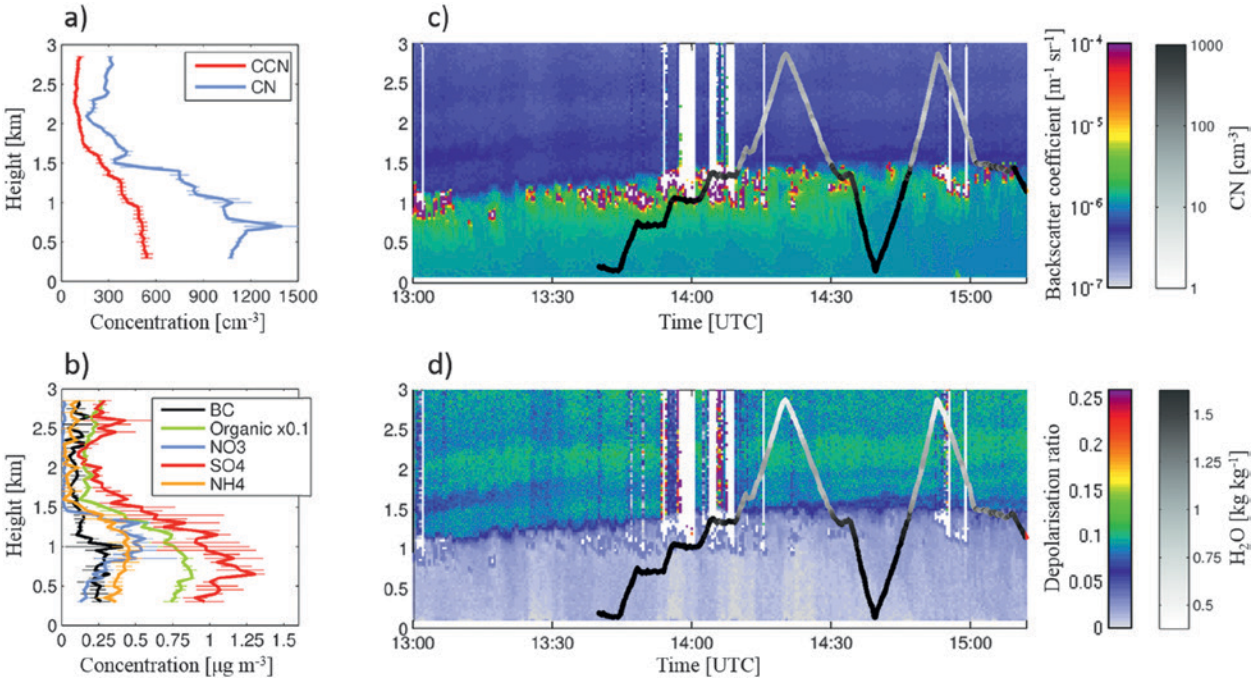

FIG. 4. (left) FMI Skyvan measurements during an aircraft IOP centered on Hyytiälä on 4 Sep 2014, showing (a) aerosol and CCN number concentration and (b) aerosol composition from Aerodyne aerosol mass spectrometer (AMS) for the first ascent leg (1340–1415 UTC). Data have been averaged to 50-m-height intervals, with thick lines displaying the mean values and thin horizontal lines indicating plus or minus one standard deviation. (right) Time–height sections of ground-based ARM HSRL (c) backscatter coefficient and (d) circular depolarization ratio data for the same day, showing the potential for aerosol-layer identification and aerosol typing. Superimposed on the HSRL plots is the Skyvan altitude track; the monochrome color of the track provides the total aerosol number concentration in (c) and the water vapor mixing ratio from Picarro in (d).

The snowfall measurement experiment (BAECC SNEX; Fig. SB1) was a collaborative effort between DOE ARM, University of Helsinki, FMI, NASA, and Colorado State University. The IOP took place from 1 February to 30 April 2014 and was dedicated to documenting snowfall microphysics through a combination of multi-frequency (C, X, Ka, and W band) radar, microwave radiometer, and lidar measurements supplemented by a comprehensive suite of surface-based precipitation observations. Combining the multi-instrumental remote sensing and ground-based observations provides a detailed view of snow growth processes, such as condensation growth of ice crystals, aggregation, and riming.

The standard AMF2 surface-based precipitation measurement instruments were supplemented by an array of sensors, given in Table SB1. The operational schedule of the nearest FMI dual-polarization weather radar was modified to include range–height indicator (RHI) scans above the AMF2 location.

To facilitate accurate surface measurements of snowfall properties, a DFIR wind protection (shown in Fig. SB1) for the following instruments was built on site: weighing precipitation gauge, laser disdrometer (OTT Parsivel), and 2D video disdrometer. Because of the duplication of the instruments, consistency of the precipitation microphysics retrievals can be checked and the dataset can also be used to characterize snowfall measurement errors as a function of wind speed. The wind measurements were performed at instrument height inside and outside of the fence and at 10-m height.

During the IOP, more than 20 precipitation events were recorded, with conditions varying from dry to wet snow and particle types ranging from pristine crystals to densely rimed particles and fluffy aggregates.

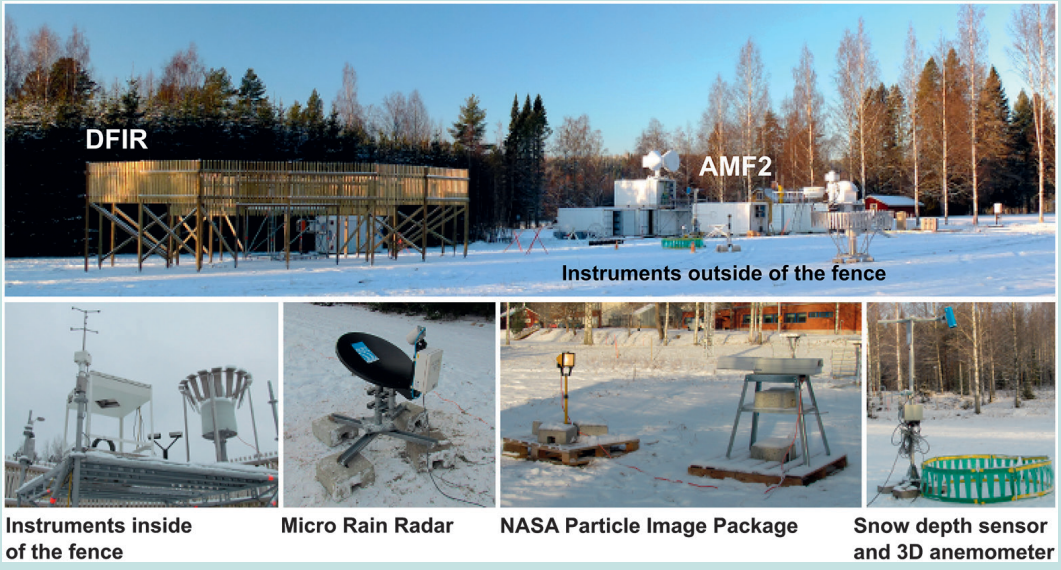

Fig. SB1. Instruments and their setup during BAECC SNEX.

Table SB1. List of BAECC SNEX instruments.

Instrument name	Inside DFIR	Outside DFIR	Measured quantities
Weighing gauge (OTT Pluvio^2)	×	×	Precipitation rate and accumulation
2D video disdrometer	×	×	PSD, fall velocity, and shape
Video disdrometer (OTT Parsivel)	×	×	PSD, fall velocity
3D anemometer (METEK and Gill)	×	×	3D wind field
Total precipitation sensor (Yankee TPS-3100)	×	—	Precipitation rate and accumulation
Particle Imaging Package (NASA)	—	×	PSD, fall velocity, fall attitude, and shape of particles
Micro Rain Radar (METEK)	—	×	Radar reflectivity and Doppler velocity (60–1000 m)
Snow depth sensor (Jenoptik SHM-30)	—	×	Snow depth

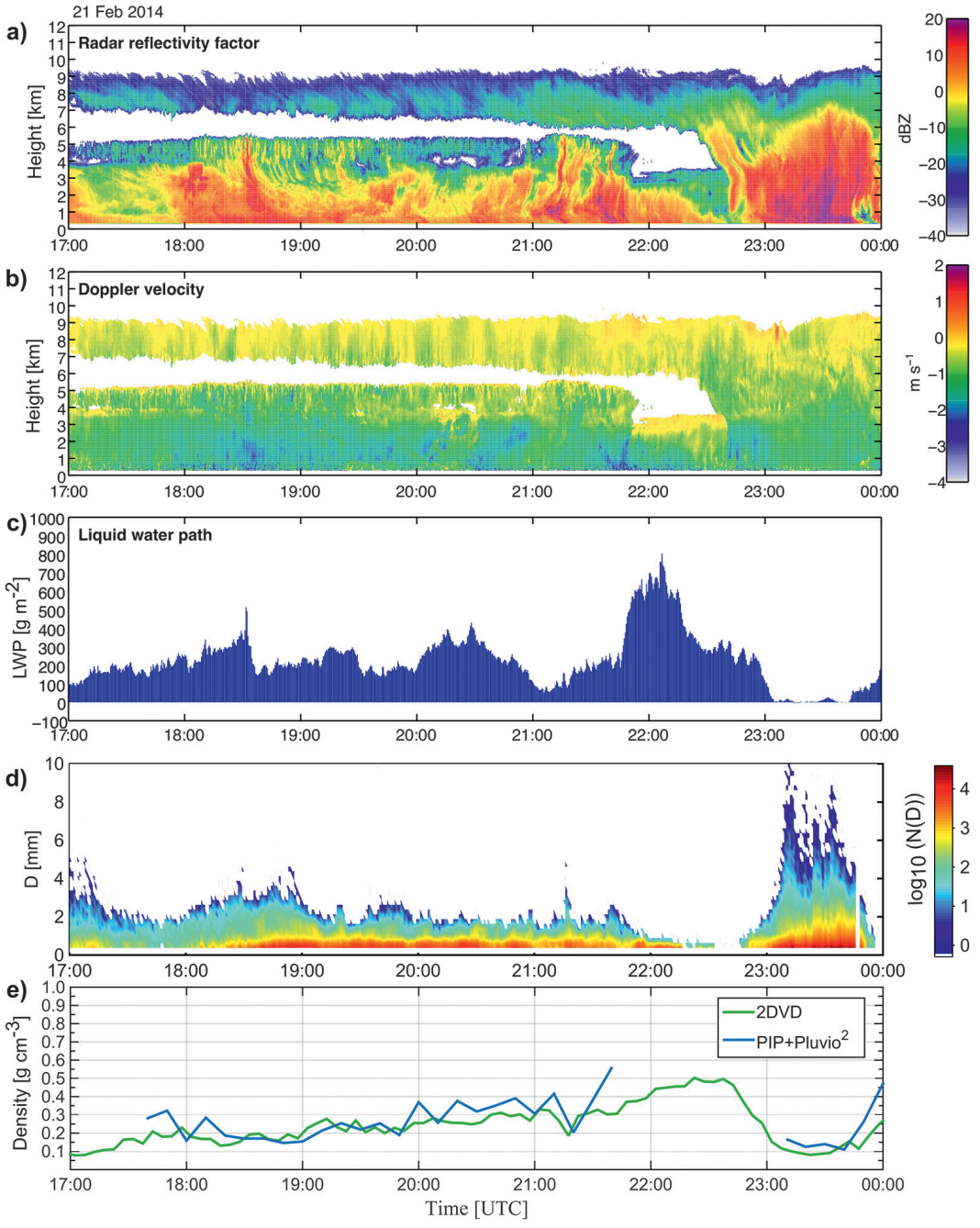

Fig. 5. KAZR observations of (a) reflectivity factor and (b) Doppler velocity, (c) MWR measurements of liquid water path (LWP), (d) particle size distribution by PIP, and (e) retrieved bulk density values. The bulk densities of snow were retrieved by applying the method of Böhm (1989) to 2D video observations and from a combination of PIP and gauge observations.

measured at the surface. Figures 3 and 4 both show suitable clouds at the top of the boundary layer that are coupled to the surface (in Fig. 3, suitable clouds are at 1.5–2 km in altitude from 1000 UTC to just after 1200 UTC; in Fig. 4, the intermittent clouds are present all day between 1 and 1.5 km). Liquid clouds in the boundary layer will be classified according to their aerosol source, biogenic, background, or other aerosol source, once these data are available and stratified by their macro- and microphysical properties to document evidence for the influence of biogenic aerosols on clouds.

CLOUDS TO PRECIPITATION. In Finland, a high-latitude country, the majority of precipitation is initiated by ice-phase processes (Mason 1971). Since

MODELING ACTIVITIES FOR INVESTIGATING AEROSOL TRANSPORT, SOURCE ATTRIBUTION, AND CLOUD-TO-PRECIPITATION PROCESSES

By combining the detailed observations obtained during BAECC with a range of numerical models, we ultimately aim to understand the role of biogenic aerosols in cloud formation and microphysical processes leading to precipitation. Here, one example is presented in which surface and remote sensing observations are combined with a numerical simulation conducted with the WRF Model, version 3.6.1 (Skamarock et al. 2008).

During BAECC SNEX (see "Clouds to precipitation" section and the "BAECC SNEX" sidebar), six cases of layered cloud that resulted in enhanced surface precipitation occurred. On 21–22 February, a frontal system that lead to multiple cloud layers and snowfall moved east across Finland. This case is analyzed in detail using WRF Model output and observations (some of which are presented in Fig. 5) to determine 1) what microphysical processes are occurring aloft and how these relate to the type and intensity of precipitation observed at the surface and 2) how accurately multiple mixed-phase cloud layers and their microphysical processes are represented by WRF.

The WRF simulation was initialized from the European Centre for Medium-Range Weather Forecasts (ECMWF) interim reanalysis (ERA-Interim) data (Dee et al. 2011) at 1200 UTC 20 February 2014 and run for 72 h. The simulation domain consisted of an outer domain with 30-km grid spacing covering most of northern Europe and an inner nested domain with 10-km grid spacing covering Finland and neighboring sea areas. Boundary layer turbulence was parameterized using the Yonsei University (YSU) scheme, deep convection was parameterized using the Kain–Fritsch scheme, and the Morrison double-moment six-class scheme was used to parameterize the microphysics. The WRF simulation did not capture the thin layer of boundary layer cloud that was present before the arrival of the front, which is, in part, due to model spinup issues, but in general such low-level clouds are poorly represented in numerical weather prediction (NWP) and climate models (Stevens et al. 2007). Associated with the frontal passage were two cloud layers, both of which were captured well by WRF (Figs. SB2 and 5).

The observed radar reflectivity (Fig. 5a) shows that between 2300 and 0000 UTC, precipitation from the upper-cloud layer falls into the lower-cloud layer. The same feature is present in the WRF simulation; however, it occurs 1.5 h later, between 0030 and

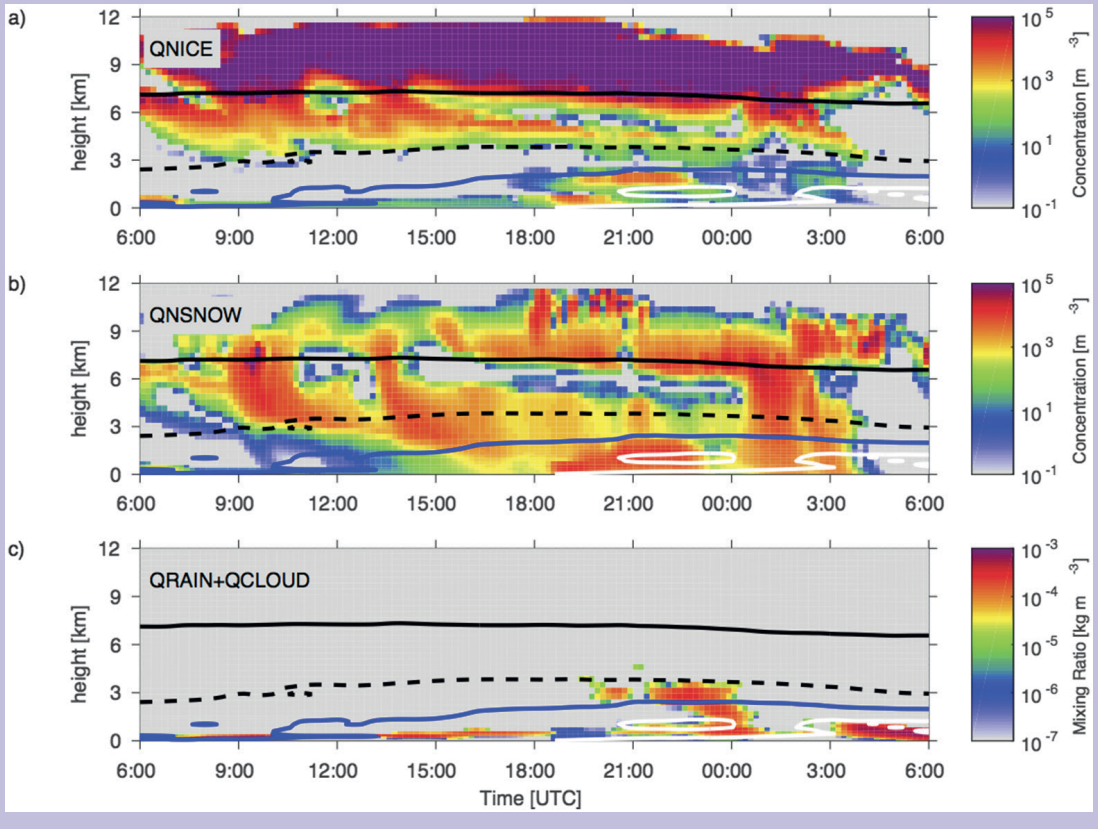

FIG. SB2. Hydrometeor properties as simulated by WRF between 0600 UTC 21 Feb and 0600 UTC 22 Feb 2014 at the grid point closest to Hyytiälä. (a) Number concentration (m^{-3}) of ice particles, (b) number concentration (m^{-3}) of snow particles, and (c) the sum of the rain and cloud mixing ratios (kg m^{-3}). The solid lines indicate temperature contours: solid black is −40°C, dashed black is −15°C, blue is −8°C, and white is −3°C.

0300 UTC (Fig. SB2). At the upper levels, where the temperature is below −40°C, there are large numbers of ice particles (Fig. SB2). These primary ice and snow particles produced in the upper-level seeder cloud fall into the lower feeder cloud and grow by accretion. Observations and model simulations of liquid and ice water path (Fig. SB3) support this as almost all liquid water is removed with the onset of the precipitation falling from the upper cloud into the lower cloud and there is an increase in ice water path (at 2300 UTC in the observations and 0030 UTC in the model simulation). In addition, new ice is generated at the top of the seeder cloud (at temperatures from −20° to −15°C) and hence would be plates or dendrites. This results in two distinct populations that have different fall speeds and therefore aggregation can readily occur. Observations (Fig. 5) show that after 2300 UTC there are more large particles and that the bulk density of snow at the surface decreases, indicative of aggregates. Thus, it can be concluded that a seeder–feeder mechanism occurs and alters the properties of the surface precipitation.

Also of interest in this case is the high concentration of ice particles simulated by WRF between 1930 and 2130 UTC at temperatures between −8° and −3°C, the temperature range where the Hallett–Mossop ice splintering processes is expected to occur (Hallett and Mossop 1974). However, in this case it is unlikely that this ice is produced by this process as there is little or no supercooled liquid present. This potential case of secondary ice production, and others observed during BAECC SNEX, will be the topic of future studies.

Overall, WRF reproduces the bulk aspects of this frontal case very well. There is reasonable agreement in the cumulative precipitation when the entire frontal system is considered, yet WRF simulates the precipitation to be lighter and to occur over a longer period of time than what was observed (Fig. SB3). Furthermore, notable discrepancies between the measured and simulated number concentration of ice/snow particles at the surface were detected (Fig. SB3) as WRF was not able to capture the increase in frozen hydrometeor number that occurred between 2300 and 0000 UTC. This highlights the challenges models face in correctly simulating precipitation amounts and properties of hydrometeors and indicates that microphysical processes are not yet adequately represented in numerical weather prediction or climate models.

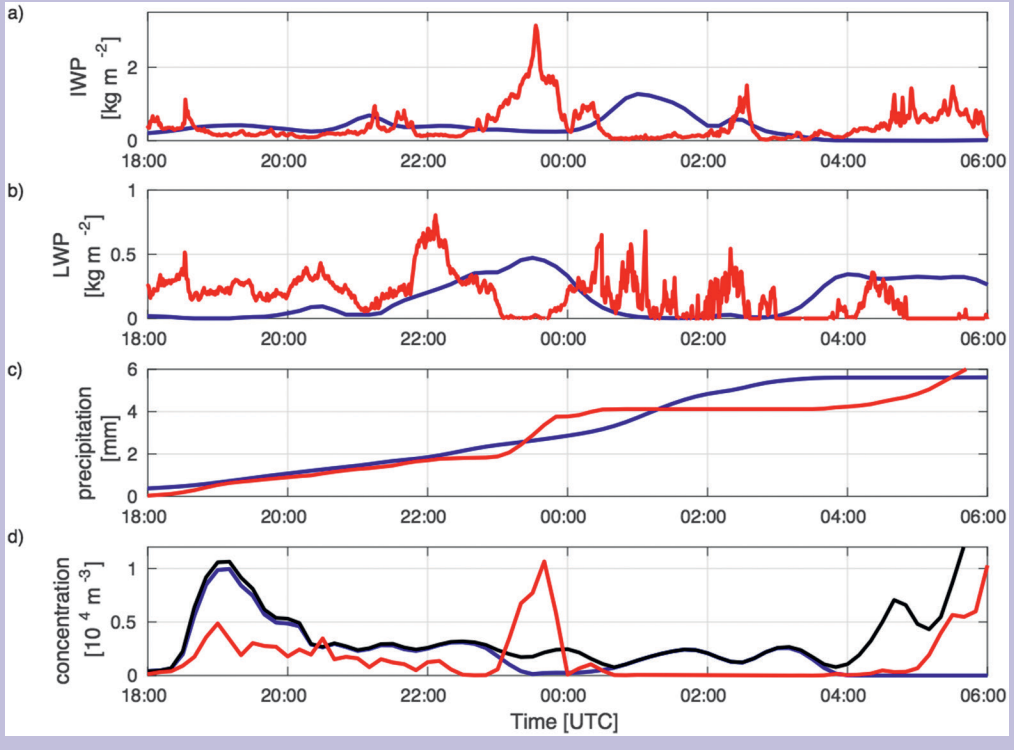

Fig. SB3. Observed (red lines) and WRF-simulated (blue lines) (a) ice water path (IWP) and (b) LWP. In WRF, LWP was calculated from the vertical integral of the sum of the cloud and rain mixing ratios, and IWP was calculated as the vertical integral of the sum of the snow, ice, and graupel mixing ratios. (c) Accumulated surface precipitation at Hyytiälä from observations (red) and WRF simulation (blue). (d) Observed total number concentration of solid precipitation particles at the surface (red), WRF-simulated total number concentration of frozen hydrometeors [snow, ice, and graupel (blue)], and WRF-simulated total number concentration [snow, ice, graupel, and rain (black)] at the lowest model level (approximately 25 m).

part of the BAECC campaign took place during winter, surface-based observations of solid precipitation microphysics, that is, particle size distribution, particle habit, and their physical properties, can be used to infer what cloud-to-precipitation processes take place and guide retrievals based on remote sensing observations. To take advantage of this opportunity, an intensive observation period termed the BAECC Snowfall Experiment (SNEX), focusing on snowfall, was undertaken from 1 February through to 30 April 2014.

During this IOP, more than 20 snowfall events were recorded. During these events, the dual-channel microwave radiometer detected the presence of liquid water more than 80% of the time. Given the presence of supercooled liquid in the majority of the cases, the focus of the IOP was to investigate how remote sensing observations, that is, multifrequency and dual-polarization Doppler radar in combination with lidar and microwave radiometer, can be used to identify ice-phase precipitation processes, namely, the Bergeron process, riming, aggregation, and ice multiplication, and study their evolution. Because a transition from one process to another could happen within a precipitation event, our analysis and data collection strategies were selected to allow investigation of how the environmental conditions influence these transitions, even if they happen on time scales as short as a few minutes.

Accurate and consistent quantitative observations of snow are notoriously challenging (Rasmussen et al. 2012). To ensure the quality of the measurements and to obtain an estimate of uncertainty of retrieved microphysical properties, a comprehensive precipitation measurement setup was established (see sidebar on "BAECC SNEX" for more information). The observations of precipitation intensity and particle size distributions, particle fall velocities and sizes, particle dimensions and shapes in combination with retrievals of snow bulk density, and mass-dimensional relations can be used for classification and characterization of precipitating ice particles and inferences of prevailing precipitation processes. These observations and retrievals were carried out in coordination with radar observations to link surface observations of precipitation microphysics to vertical profiles of meteorological products, as, for example, shown in Kneifel et al. (2015). An example of this analysis applied to a precipitation event that took place on 21 February 2014 is shown in Fig. 5. Furthermore, in the sidebar "Modeling activities for investigating aerosol transport, source attribution, and cloud-to-precipitation processes," an example of how a numerical model—the Weather Research and Forecasting (WRF) Model—can be used to further understand how microphyiscal processes occurring in a vertical column affect the properties of precipitation at the surface is presented.

During BAECC SNEX, surface precipitation observations were performed by a number of instruments. Given the duplication of most of the precipitation instruments and utilization of instruments with different measurement principles, the consistency of the retrieved snow microphysical properties can be checked. For example, precipitation intensity is measured by two weighing gauges [inside and outside of the Double Fence Intercomparison Reference (DFIR)] and by a total precipitation sensor (Hotplate). Those instruments supplement standard AMF instrumentation. Particle size distributions were recorded by two OTT Parsivel laser disdrometers, two 2D video disdrometers, and a particle imaging package (PIP) designed by the National Aeronautics and Space Administration (NASA), which is the new generation of snow video imager, providing also images of individual hydrometeors (Newman et al. 2009).

Similarly, retrieval techniques that rely on different sets of assumptions were adopted. To characterize precipitating ice particles, bulk density of falling snow, velocity–dimensional (v–D) relations, areal ratios, and mass–dimensional (m–D) relations must be derived. The bulk density can, for example, be estimated using several methods:

- by matching 2D video and/or PIP-based estimates of snowfall rate to the value recorded by the gauges, similar to the techniques described by Brandes et al. (2007);
- estimating the bulk density of freshly fallen snow by comparing changes in snow depth to the precipitation accumulation (Power et al. 1964); and
- by matching reflectivity values calculated from PSD observations with directly observed reflectivity values (Huang et al. 2010).

An example of retrieved bulk density values from PIP and weighing-gauge measurements is shown in Fig. 5. By combining observed particle area ratios and v–D relations, the mass-dimensional relations were estimated by following the procedure described by Böhm (1989) and Huang et al. (2015); see Fig. 5 for the bulk density calculated from the retrieved m–D relation. As one can see from Fig. 5, the bulk densities retrieved using two different sets of instruments and methods match rather well, which supports our confidence that such retrievals are possible and meaningful.

SUMMARY AND OUTLOOK. During BAECC, the physical, chemical, and optical characterization of aerosol particles at the surface was conducted simultaneously with comprehensive cloud and precipitation observations. This was enabled by combining the state-of-the-art capabilities of both the SMEAR II research station at Hyytiälä, Finland, and the AMF2, a mobile research facility, which was brought to Hyytiälä by the ARM Program of the U.S. Department of Energy. This facilitated good opportunities to benefit from the NASA Global Precipitation Measurement (GPM) mission ground validation in surface particle size distribution and water equivalent rate gauges, while the European Commission via ACTRIS transnational access provided resources for gap-filling aerosol physical and chemical measurements as well as cloud observations.

Overall, the BAECC campaign was highly successful and provided a vast 8-month-long dataset obtained during three seasons, including a variety of cloud and precipitation systems. Together with the extensive flight campaigns, and with the comprehensive near-20-yr-long continuous surface-based measurements of aerosols at SMEAR II, the representativeness of the BAECC dataset can be thoroughly evaluated.

The connection between increased aerosol concentration of aerosol particles and cloud properties has not yet been properly quantified because of the challenges connecting in situ aerosol measurements at the ground and cloud properties aloft (e.g., Paasonen et al. 2013 ; Kulmala et al. 2014). With vertical profile measurements during BAECC and suitable modeling tools, the quantification of these connections can now be undertaken. The comprehensive observations available in BAECC enable radiative transfer modeling to estimate the effects of aerosols and clouds on the radiative (e.g. Zieger et al. 2015) energy balance of the entire atmospheric column. With the combination of the measurements obtained during BAECC and the supporting SMEAR network, combined with satellite data, we will be able to evaluate these correlations on a larger spatial scale in the boreal environment.

Expansion of the pointwise measurements to a larger context with satellite-derived data is ongoing (Sporre et al. 2016; Krüger et al. 2016, manuscript submitted to *J. Geophys. Res.*). The data will enable development of proxy variables that can be expanded into a global perspective (e.g., Kulmala et al. 2011).

The comprehensive data will be utilized in multiscale modeling. For example, the atmosphere column model SOSAA (Boy et al. 2011), combining different emission modules, boundary layer dynamics, and both chemical and aerosol dynamical processes, will be used to investigate the formation, vertical transport, and aging of atmospheric aerosols inside the mixing layer. The model simulations will link our knowledge based on long-term ground observation with the new measurements by the AMF instruments. Valuable sensitivity studies with the Weather Research and Forecasting Model with Chemistry (WRF-Chemistry) with different cloud microphysics parameterizations are possible where the models can be verified against multifrequency radar observations available from AMF2.

Future work will take full advantage of the success of the BAECC campaign and contribute toward the following objectives: 1) to study the interactions between aerosol microphysics and turbulent mixing within the continental boundary layer to understand the transformation of aerosol while being transported from the surface to clouds, 2) to evaluate the impacts of long-range transport and transformation of aerosol on how they can act as CCN, 3) through comprehensive aerosol typing with the various observation methods to determine the roles of the regional and long-range transported aerosol in the formation of CCN-sized particles, 4) to investigate the sensitivity of evolving cloud–precipitation processes on CCN concentrations, 5) to characterize aerosol removal and transformation mechanisms as a function of particle size and precipitation type, and 6) to compare and understand falling-snow precipitation processes and rates to remote sensing retrievals from satellite missions such as GPM.

Finally, the representativeness of the BAECC data will be understood within a long-term perspective through connection to the nearly 20-yr continuous measurement dataset at SMEAR II, unique globally in the sense that nowhere else has comparable measurements that have been performed continuously for such a long time period.

ACKNOWLEDGMENTS. This work was partly supported by the Office of Science (BER), U.S. Department of Energy via BAECC (Petäjä), BAECC SNEX (Moisseev), DE-SC0011791 (Thornton), DE-SC0014469 (Smith), and ASR (Chandrasekar); European Commission via projects ACTRIS, ACTRIS-TNA, ACTRIS2, BACCHUS, and PEGASOS and European Research Council via NANODYNAMITE (616075); and Academy of Finland Centre of Excellence (Project 272041), KONE foundation (Grant 46-6817), Nordforsk via Cryosphere–Atmosphere Interactions in a Changing Arctic Climate, CRAICC, TEKES in the CLEEN/MMEA programme, and the Ministry of Transport and Communication through ICOS-Finland. The BAECC SNEX was also supported by NASA Global Precipitation Measurement (GPM) mission ground validation program.

The deployment of AMF2 to Hyytiälä was enabled and supported by ARM. Argonne National Laboratory's work was supported by the U.S. Department of Energy, Assistant Secretary for Environmental Management, Office of Science and Technology, under Contract DE-AC02-06CH11357. The authors gratefully acknowledge the support of AMF2, SMEAR II, and the BAECC community for their support in initiating the BAECC campaign, its implementation, operation, and data analysis.

REFERENCES

Aalto, J., and Coauthors, 2014: New foliage growth is a significant, unaccounted source for volatiles in boreal evergreen forests. *Biogeosciences*, **11**, 1331–1344, doi:10.5194/bg-11-1331-2014.

——, and Coauthors, 2015: Onset of photosynthesis in spring speeds up monoterpene synthesis and leads to emission bursts. *Plant Cell Environ.*, **38**, 2299–2312, doi:10.1111/pce.12550.

Aaltonen, H., J. Pumpanen, M. Pihlatie, H. Hakola, H. Hellén, L. Kulmala, T. Vesala, and J. Bäck, 2011: Boreal pine forest floor biogenic volatile organic compound emissions peak in early summer and autumn. *Agric. For. Meteor.*, **151**, 682–691, doi:10.1016/j.agrformet.2010.12.010.

Ahmad, I., and Coauthors, 2013: Long-term measurements of cloud droplet concentrations and aerosol–cloud interactions in continental boundary layer clouds. *Tellus*, **65B**, 20138, doi:10.3402/tellusb.v65i0.20138.

Almeida, J., and Coauthors, 2013: Molecular understanding of sulphuric acid–amine particle nucleation in the atmosphere. *Nature*, **502**, 359–363, doi:10.1038/nature12663.

Althausen, D., R. Engelmann, H. Baars, B. Heese, A. Ansmann, D. Müller, and M. Komppula, 2009: Portable Raman lidar Polly^{XT} for automated profiling of aerosol backscatter, extinction, and depolarization. *J. Atmos. Oceanic Technol.*, **26**, 2366–2378, doi:10.1175/2009JTECHA1304.1.

ARM, 2015: ARM data archive. ARM Climate Research Facility, accessed 22 October 2015. [Available online at www.archive.arm.gov/armlogin/login.jsp.]

Atkinson, R., and J. Arey, 2003: Gas-phase tropospheric chemistry of biogenic volatile organic compounds: A review. *Atmos. Environ.*, **37**, 197–219, doi:10.1016/S1352-2310(03)00391-1.

Bäck, J., J. Aalto, M. Henriksson, H. Hakola, Q. He, and M. Boy, 2012: Chemodiversity of a Scots pine stand and implications for terpene air concentrations. *Biogeosciences*, **9**, 689–702, doi:10.5194/bg-9-689-2012.

Barlow, J. F., T. M. Dunbar, E. G. Nemitz, C. R. Wood, M. W. Gallagher, F. Davies, E. O'Connor, and R. M. Harrison, 2011: Boundary layer dynamics over London, UK, as observed using Doppler lidar during REPARTEE-II. *Atmos. Chem. Phys.*, **11**, 2111–2125, doi:10.5194/acp-11-2111-2011.

Binietoglou, I., and Coauthors, 2015: A methodology for investigating dust model performance using synergistic EARLINET/AERONET dust concentration retrievals. *Atmos. Meas. Tech.*, **8**, 3577–3600, doi:10.5194/amt-8-3577-2015.

Böhm, H. P., 1989: A general equation for the terminal fall speed of solid hydrometeors. *J. Atmos. Sci.*, **46**, 2419–2427, doi:10.1175/1520-0469(1989)046<2419:AGEFTT>2.0.CO;2.

Bonan, G. B., 2008: Forests and climate change: Forcings, feedbacks, and the climate benefits of forests. *Science*, **320**, 1444–1449, doi:10.1126/science.1155121.

Boucher, O., and Coauthors, 2013: Clouds and aerosols. *Climate Change 2013: The Physical Science Basis*, T. F. Stocker et al., Eds., Cambridge University Press, 571–657.

Boy, M., A. Sogachev, J. Lauros, L. Zhou, A. Guenther, and S. Smolander, 2011: SOSA—A new model to simulate the concentrations of organic vapours and sulphuric acid inside the ABL—Part 1: Model description and initial evaluation. *Atmos. Chem. Phys.*, **11**, 43–51, doi:10.5194/acp-11-43-2011.

Brandes, E. A., K. Ikeda, G. Zhang, M. Schönhuber, and R. M. Rasmussen, 2007: A statistical and physical description of hydrometeor distributions in Colorado snowstorms using a video disdrometer. *J. Appl. Meteor. Climatol.*, **46**, 634–650, doi:10.1175/JAM2489.1.

Carslaw, K. S., and Coauthors, 2013: Large contribution of natural aerosols to uncertainty in indirect forcing. *Nature*, **503**, 67–71, doi:10.1038/nature12674.

Chaikovsky, A., and Coauthors, 2016: Lidar-Radiometer Inversion Code (LIRIC) for the retrieval of vertical aerosol properties from combined lidar/radiometer data: development and distribution in EARLINET, *Atmos. Meas. Tech.*, **9**, 1181–1205, doi:10.5194/amt-9-1181-2016.

Dal Maso, M., M. Kulmala, I. Riipinen, R. Wagner, T. Hussein, P. P. Aalto, and K. E. J. Lehtinen, 2005: Formation and growth of fresh atmospheric aerosols: Eight years of aerosol size distribution data from SMEAR II, Hyytiälä, Finland. *Boreal Environ. Res.*, **10**, 323–336.

——, P. Hari, and M. Kulmala, 2009: Spring recovery of photosynthesis and atmospheric particle formation. *Boreal Environ. Res.*, **14**, 711–721.

DeCarlo, P.F., and Coauthors, 2006: Field-deployable, high-resolution, time-of-flight aerosol mass spectrometer. *Anal. Chem.*, **78**, 8281–8289, doi:10.1021/ac061249n.

Dee, D. P., and Coauthors, 2011: The ERA-Interim reanalysis: Configuration and performance of the data assimilation system. *Quart. J. Roy. Meteor. Soc.*, **137**, 553–597, doi:10.1002/qj.828.

Ehn, M., and Coauthors, 2010: Composition and temporal behavior of ambient ions in the boreal forest. *Atmos. Chem. Phys.*, **10**, 8513–8530, doi:10.5194/acp-10-8513-2010.

——, and Coauthors, 2014: A large source of low-volatility secondary organic aerosol. *Nature*, **506**, 476–479, doi:10.1038/nature13032.

Emeis, S., K. Schäfer, and C. Münkel, 2008: Surface-based remote sensing of the mixing-layer height—A review. *Meteor. Z.*, **17**, 621–630, doi:10.1127/0941-2948/2008/0312.

Engelmann, R., and Coauthors, 2016: The automated multiwavelength Raman polarization and water-vapor lidar Polly^{XT}: The neXT generation. *Atmos. Meas. Tech.*, **9**, 1767–1784, doi:10.5194/amt-9-1767-2016.

Epstein, H. E., I. Myers-Smith, and D. A. Walker, 2013: Recent dynamics of arctic and sub-arctic vegetation. *Environ. Res. Lett.*, **8**, 015040, doi:10.1088/1748-9326/8/1/015040.

Ghirardo, A., K. Koch, R. Taipale, I. Zimmer, J.-P. Schnitzler, and J. Rinne, 2010: Determination of *de novo* and pool emissions of terpenes from four common boreal/alpine trees by $^{13}CO_2$ labelling and PTR-MS analysis. *Plant Cell Environ.*, **33**, 781–792, doi:10.1111/j.1365-3040.2009.02104.x.

Guenther, A., and Coauthors, 1995: A global model of natural volatile organic compound emission. *J. Geophys. Res.*, **100**, 8873–8892, doi:10.1029/94JD02950.

Häkkinen, S. A. K., and Coauthors, 2012: Long-term volatility measurements of submicron atmospheric aerosol in Hyytiälä, Finland. *Atmos. Chem. Phys.*, **12**, 10 771–10 786, doi:10.5194/acp-12-10771-2012.

Hakola, H., V. Tarvainen, J. Bäck, H. Ranta, B. Bonn, J. Rinne, and M. Kulmala, 2006: Seasonal variation of mono- and sesquiterpene emission rates of Scots pine. *Biogeosciences*, **3**, 93–101, doi:10.5194/bg-3-93-2006.

Hallett, J., and S. C. Mossop, 1974: Production of secondary ice particles during the riming process. *Nature*, **249**, 26–28, doi:10.1038/249026a0.

Hari, P., and M. Kulmala, 2005: Station for Measuring Ecosystem–Atmosphere Relations (SMEAR II). *Boreal Environ. Res.*, **10**, 315–322.

Huang, G.-J., V. N. Bringi, R. Cifelli, D. Hudak, and W. A. Petersen, 2010: A methodology to derive radar reflectivity–liquid equivalent snow rate relations using C-band radar and a 2D video disdrometer. *J. Atmos. Oceanic Technol.*, **27**, 637–651, doi:10.1175/2009JTECHA1284.1.

——, ——, D. Moisseev, W. A. Petersen, L. Bliven, and D. Hudak, 2015: Use of 2D-video disdrometer to derive mean density–size and Z_e–SR relations: Four snow cases from the light precipitation validation experiment. *Atmos. Res.*, **153**, 34–48, doi:10.1016/j.atmosres.2014.07.013.

Illingworth, A. J., and Coauthors, 2007: CLOUDNET: Continuous evaluation of cloud profiles in seven operational models using ground-based observations. *Bull. Amer. Meteor. Soc.*, **88**, 883–898, doi:10.1175/BAMS-88-6-883.

Jefferson, A., 2011: Aerosol Observing System (AOS) handbook. U.S. Department of Energy, Office of Science, Office of Biological and Environmental Research Tech. Rep. DOE/SC-ARM/TR-014, 32 pp.

Jimenez, J. L., and Coauthors, 2009: Evolution of organic aerosols in the atmosphere. *Science*, **326**, 1525–1529, doi:10.1126/science.1180353.

Jokinen, T., and Coauthors, 2012: Atmospheric sulphuric acid and neutral cluster measurements using CI-APi-TOF. *Atmos. Chem. Phys.*, **12**, 4117–4125, doi:10.5194/acp-12-4117-2012.

Junninen, H., A. Lauri, P. Keronen, P. Aalto, V. Hiltunen, P. Hari, and M. Kulmala, 2009: Smart-SMEAR: on-line data exploration and visualization tool for SMEAR stations. *Boreal Environ. Res.*, **14**, 447–457.

——, and Coauthors, 2010: A high-resolution mass spectrometer to measure atmospheric ion composition. *Atmos. Meas. Tech.*, **3**, 1039–1053, doi:10.5194/amt-3-1039-2010.

Kauppi, P., P. Anttila, and K. Kenttämies, Eds., 1990: *Acidification in Finland*. Springler-Verlag, 1237 pp.

Kerminen, V.-M., H. Lihavainen, M. Komppula, Y. Viisanen, and M. Kulmala, 2005: Direct observational evidence linking atmospheric aerosol formation and cloud droplet activation. *Geophys. Res. Lett.*, **32**, L14803, doi:10.1029/2005GL023130.

——, and Coauthors, 2012: Cloud condensation nuclei production associated with atmospheric nucleation: A synthesis based on existing literature and new results. *Atmos. Chem. Phys.*, **12**, 12 037–12 059, doi:10.5194/acp-12-12037-2012.

Kirkby, J., and Coauthors, 2011: Role of sulfuric acid, ammonia and galactic cosmic rays in atmospheric aerosol nucleation. *Nature*, **476**, 429–433, doi:10.1038/nature10343.

——, and Coauthors, 2016: Ion-induced nucleation of pure biogenic particles. *Nature*, **533**, 521–526, doi:10.1038/nature17953.

Kneifel, S., A. von Lerber, J. Tiira, D. Moisseev, P. Kollias, and J. Leinonen, 2015: Observed relations between snowfall microphysics and triple-frequency radar measurements. *J. Geophys. Res. Atmos.*, **120**, 6034–6055, doi:10.1002/2015JD023156.

Koenigk, T., L. Brodeau, R. G. Graversen, J. Karlsson, G. Svensson, M. Tjernström, U. Willén, and K. Wyser,

2013: Arctic climate change in 21st century CMIP5 simulations with EC-Earth. *Climate Dyn.*, **40**, 2719–2743, doi:10.1007/s00382-012-1505-y.

Kulmala, M., A. Toivonen, J. M. Mäkelä, and A. Laaksonen, 1998: Analysis of the growth of nucleation mode particles observed in Boreal forest. *Tellus*, **50B**, 449–462, doi:10.1034/j.1600-0889.1998.t01-4-00004.x.

——, and Coauthors, 2001: On the formation, growth and composition of nucleation mode particles. *Tellus*, **53B**, 479–490, doi:10.3402/tellusb.v53i4.

——, H. Vehkamäki, T. Petäjä, M. Dal Maso, A. Lauri, V.-M. Kerminen, W. Birmili, and P. H. McMurry, 2004: Formation and growth rates of ultrafine atmospheric particles: A review of observations. *J. Aerosol Sci.*, **35**, 143–176, doi:10.1016/j.jaerosci.2003.10.003.

——, and Coauthors, 2007: Toward direct measurement of atmospheric nucleation. *Science*, **318**, 89–92, doi:10.1126/science.1144124.

——, A. Arola, T. Nieminen, L. Riuttanen, L. Sogacheva, G. de Leeuw, V.-M. Kerminen, and K. E. J. Lehtinen, 2011: First estimates of global nucleation mode aerosol concentrations based on satellite measurements. *Atmos. Chem. Phys.*, **11**, 10 791–10 801, doi:10.5194/acp-11-10791-2011.

——, and Coauthors, 2013: Direct observations of atmospheric aerosol nucleation. *Science*, **339**, 943–946, doi:10.1126/science.1227385.

——, and Coauthors, 2014: CO_2 induced terrestrial climate feedback mechanism: From carbon sink to aerosol source and back. *Boreal Environ. Res.*, **19B**, 122–131.

Lopatin, A., O. Dubovik, A. Chaikovsky, P. Goloub, T. Lapyonok, D. Tanré, and P. Litvinov, 2013: Enhancement of aerosol characterization using synergy of lidar and sun-photometer coincident observations: The GARRLiC algorithm. *Atmos. Meas. Tech.*, **6**, 2065–2088, doi:10.5194/amt-6-2065-2013.

Lopez-Hilfiker, F. D., and Coauthors, 2014: A novel method for online analysis of gas and particle composition: Description and evaluation of a Filter Inlet for Gases and AEROsols (FIGAERO). *Atmos. Meas. Tech.*, **7**, 983–1001, doi:10.5194/amt-7-983-2014.

Mäkelä, J., and Coauthors, 1997: Observations of ultrafine aerosol particle formation and growth in boreal forest. *Geophys. Res. Lett.*, **24**, 1219–1222, doi:10.1029/97GL00920.

Mason, B. J., 1971: *The Physics of Clouds*. 2nd ed. Clarendon Press, 671 pp.

Mattis, I., A. Ansmann, D. Müller, U. Wandinger, and D. Althausen, 2004: Multilayer aerosol observations with dual-wavelength Raman lidar in the framework of EARLINET. *J. Geophys. Res.*, **109**, D13203, doi:10.1029/2004JD004600.

Merikanto, J., D. V. Spracklen, G. W. Mann, S. J. Pickering, and K. S. Carslaw, 2009: Impact of nucleation on global CCN. *Atmos. Chem. Phys.*, **9**, 8601–8616, doi:10.5194/acp-9-8601-2009.

Mikkonen, S., and Coauthors, 2011: A statistical proxy for sulphuric acid concentration. *Atmos. Chem. Phys.*, **11**, 11 319–11 334, doi:10.5194/acp-11-11319-2011.

Mona, L., A. Amodeo, G. D'Amico, A. Giunta, F. Madonna, and G. Pappalardo, 2012: Multi-wavelength Raman lidar observations of the Eyjafjallajökull volcanic cloud over Potenza, southern Italy. *Atmos. Chem. Phys.*, **12**, 2229–2244, doi:10.5194/acp-12-2229-2012.

Müller, D., U. Wandinger, and A. Ansmann, 1999: Microphysical particle parameters from extinction and backscatter lidar data by inversion with regularization: theory. *Appl. Opt.*, **38**, 2346–2357, doi:10.1364/AO.38.002346.

——, A. Ansmann, I. Mattis, M. Tesche, U. Wandinger, D. Althausen, and G. Pisani, 2007: Aerosol-type-dependent lidar ratios observed with Raman lidar. *J. Geophys. Res.*, **112**, D16202, doi:10.1029/2006JD008292.

Newman, A. J., P. A. Kucera, and L. F. Bliven, 2009: Presenting the Snowflake Video Imager (SVI). *J. Atmos. Oceanic Technol.*, **26**, 167–179, doi:10.1175/2008JTECHA1148.1.

Ng, N. L., and Coauthors, 2011: An Aerosol Chemical Speciation Monitor (ACSM) for routine monitoring of the composition and mass concentrations of ambient aerosol. *Aerosol Sci. Technol.*, **45**, 780–794, doi:10.1080/02786826.2011.560211.

Nygren, P., P. Hari, T. Raunemaa, M. Kulmala, S. Luokkanen, M. Holmberg, and E. Nikinmaa, 1994: Behaviour of ^{137}Cs from Chernobyl fallout in a Scots pine canopy in southern Finland. *Can. J. For. Res.*, **24**, 1210–1215, doi:10.1139/x94-159.

O'Connor, E. J., R. J. Hogan, and A. J. Illingworth, 2005: Retrieving stratocumulus drizzle parameters using Doppler radar and lidar. *J. Appl. Meteor.*, **44**, 14–27, doi:10.1175/JAM-2181.1.

——, A. J. Illingworth, I. M. Brooks, C. D. Westbrook, R. J. Hogan, F. Davies, and B. J. Brooks, 2010: A method for estimating the turbulent kinetic energy dissipation rate from a vertically pointing Doppler lidar, and independent evaluation from balloon-borne in situ measurements. *J. Atmos. Oceanic Technol.*, **27**, 1652–1664, doi:10.1175/2010JTECHA1455.1.

Paasonen, P., and Coauthors, 2013: Warming-induced increase in aerosol number concentration likely to moderate climate change. *Nat. Geosci.*, **6**, 438–442, doi:10.1038/ngeo1800.

Pappalardo, G., and Coauthors, 2014: EARLINET: Towards an advanced sustainable European aerosol lidar network. *Atmos. Meas. Tech.*, **7**, 2389–2409, doi:10.5194/amt-7-2389-2014.

Petäjä, T., 2013: Science plan: Biogenic Aerosols—Effects on Clouds and Climate (BAECC). U.S. Department of Energy, Office of Science, Office of Biological and Environmental Research Tech. Rep. DOE/SC-ARM-13-024, 36 pp.

——, and Coauthors, 2009: Sulfuric acid and OH concentrations in a boreal forest site. *Atmos. Chem. Phys.*, **9**, 7435–7448, doi:10.5194/acp-9-7435-2009.

——, and Coauthors, 2011: Experimental observation of strongly bound dimers of sulfuric acid: Application to nucleation in the atmosphere. *Phys. Rev. Lett.*, **106**, 228302, doi:10.1103/PhysRevLett.106.228302.

Pinterich, T., and Coauthors, 2016: The versatile size analyzing nuclei counter (vSANC). *Aerosol Sci. Technol.*, **50**, 947–958, doi:10.1080/02786826.2016.1210783.

Power, B. A., P. W. Summers, and J. D'Avignon, 1964: Snow crystal forms and riming effects as related to snowfall density and general storm conditions. *J. Atmos. Sci.*, **21**, 300–305, doi:10.1175/1520-0469(1964)021<0300:SCFARE>2.0.CO;2.

Rasmussen, R., and Coauthors, 2012: How well are we measuring snow: The NOAA/FAA/NCAR winter precipitation test bed. *Bull. Amer. Meteor. Soc.*, **93**, 811–829, doi:10.1175/BAMS-D-11-00052.1.

Raunemaa, T., S. Lehtinen, H. Saari, and M. Kulmala, 1987: 2–10 μm sized hot particles in Chernobyl fallout to Finland. *J. Aerosol Sci.*, **18**, 693–696, doi:10.1016/0021-8502(87)90099-1.

Ren, L., P. Arkin, T. M. Smith, and S. S. Shen, 2013: Global precipitation trends in 1900–2005 from a reconstruction and coupled model simulations. *J. Geophys. Res. Atmos.*, **118**, 1679–1689, doi:10.1002/jgrd.50212.

Riccobono, F., and Coauthors, 2014: Oxidation products of biogenic emissions contribute to nucleation of atmospheric particles. *Science*, **344**, 717–721, doi:10.1126/science.1243527.

Riipinen, I., and Coauthors, 2011: Organic condensation: A vital link connecting aerosol formation to cloud condensation nuclei (CCN) concentrations. *Atmos. Chem. Phys.*, **11**, 3865–3878, doi:10.5194/acp-11-3865-2011.

——, T. Yli-Juuti, J. R. Pierce, T. Petäjä, D. R. Worsnop, M. Kulmala, and N. M. Donahue, 2012: The contribution of organics to atmospheric nanoparticle growth. *Nat. Geosci.*, **5**, 453–458, doi:10.1038/ngeo1499.

Rosenfeld, D., U. Lohmann, G. B. Raga, C. D. O'Dowd, M. Kulmala, S. Fuzzi, A. Reissell, and M. O. Andreae, 2008: Flood or drought: How do aerosols affect precipitation? *Science*, **321**, 1309–1313, doi:10.1126/science.1160606.

Schobesberger, S., and Coauthors, 2013a: Molecular understanding of atmospheric particle formation from sulfuric acid and large oxidized organic molecules. *Proc. Natl. Acad. Sci. USA*, **110**, 17 223–17 228, doi:10.1073/pnas.1306973110.

——, and Coauthors, 2013b: Airborne measurements over the boreal forest of southern Finland during new particle formation events in 2009 and 2010. *Boreal Environ. Res.*, **18**, 145–163.

Sipilä, M., and Coauthors, 2010: The role of sulfuric acid in atmospheric nucleation. *Science*, **327**, 1243–1246, doi:10.1126/science.1180315.

Skamarock, W. C., and Coauthors, 2008: A description of the Advanced Research WRF version 3. NCAR Tech. Note NCAR/TN-475+STR, 113 pp., doi:10.5065/D68S4MVH.

smartSMEAR, 2016: SMEAR data archive. Accessed 27 August 2016. [Available online at www.atm.helsinki.fi/smartSMEAR/.]

Smith, J. N., K. Moore, P. McMurry, and F. Eisele, 2004: Atmospheric measurements of sub-20 nm diameter particle chemical composition by thermal desorption chemical ionization mass spectrometry. *Aerosol Sci. Technol.*, **38**, 100–110, doi:10.1080/02786820490249036.

——, M. J. Dunn, T. M. VanReken, K. Iida, M. R. Stolzenburg, P. H. McMurry, and L. G. Huey, 2008: Chemical composition of atmospheric nanoparticles formed from nucleation in Tecamac, Mexico: Evidence for an important role for organic species in nanoparticle growth. *Geophys. Res. Lett.*, **35**, L04808, doi:10.1029/2007GL032523.

——, and Coauthors, 2010: Observations of aminium salts in atmospheric nanoparticles and possible climatic implications. *Proc. Natl. Acad. Sci. USA*, **107**, 6634–6639, doi:10.1073/pnas.0912127107.

Sporre, M.K., E. J. O'Connor, N. Håkansson, A. Thoss, E. Swietlicki and T. Petäjä, 2016: Comparison of MODIS and VIIRS cloud properties with ARM ground-based observations over Finland. *Atmos. Meas. Technol.*, **9**, 3193–3203, doi:10.5194/amt-9-3193-2016.

Stephens, G. L., and C. D. Kummerow, 2007: The remote sensing of clouds and precipitation from space: A review. *J. Atmos. Sci.*, **64**, 3742–3765, doi:10.1175/2006JAS2375.1.

Stevens, B., and G. Feingold, 2009: Untangling aerosol effects on clouds and precipitation in a buffered system. *Nature*, **461**, 607–613, doi:10.1038/nature08281.

——, A. Beljaars, S. Bordoni, C. Holloway, M. Köhler, S. Krueger, V. Savic-Jovcic, and Y. Zhang, 2007: On the structure of the lower troposphere in the summertime stratocumulus regimes of the northeast Pacific. *Mon. Wea. Rev.*, **135**, 985–1005, doi:10.1175/MWR3427.1.

Taipale, R., and Coauthors, 2014: New instrument for measuring atmospheric concentrations of non-OH oxidants of SO_2. *Boreal Environ Res.*, **19**, 55–70.

Tröstl, J., and Coauthors, 2016: The role of low-volatility organic compounds in initial particle growth in the atmosphere. *Nature*, **533**, 527–533, doi:10.1038/nature18271.

Tunved, P., and Coauthors, 2006: High natural aerosol loading over boreal forests. *Science*, **312**, 261–263, doi:10.1126/science.1123052.

Vakkari, V., E. J. O'Connor, A. Nisantzi, R. E. Mamouri, and D. G. Hadjimitsis, 2015: Low-level mixing height detection in coastal locations with a scanning Doppler lidar. *Atmos. Meas. Tech.*, **8**, 1875–1885, doi:10.5194/amt-8-1875-2015.

Vanhanen, J., J. Mikkilä, K. Lehtipalo, M. Sipilä, H. E. Manninen, E. Siivola, T. Petäjä, and M. Kulmala, 2011: Particle size magnifier for nano-CN detection. *Aerosol Sci. Technol.*, **45**, 533–542, doi:10.1080/02786826.2010.547889.

Veselovskii, I., A. Kolgotin, D. Müller, and D. N. Whiteman, 2005: Information content of multiwavelength lidar data with respect to microphysical particle properties derived from eigenvalue analysis. *Appl. Opt.*, **44**, 5292–5303, doi:10.1364/AO.44.005292.

Virtanen, A., and Coauthors, 2011: Bounce behavior of freshly nucleated biogenic secondary organic aerosol particles. *Atmos. Chem. Phys.*, **11**, 8759–8766, doi:10.5194/acp-11-8759-2011.

Weber, R. J., P. H. McMurry, F. L. Eisele, and D. J. Tanner, 1995: Measurement of expected nucleation precursor species and 3-500-nm diameter particles at Mauna Loa Observatory, Hawaii. *J. Atmos. Sci.*, **52**, 2242–2257, doi:10.1175/1520-0469(1995)052<2242:MOENPS>2.0.CO;2.

Yassaa, N., W. Song, J. Lelieveld, A. Vanhatalo, J. Bäck, and J. Williams, 2012: Diel cycles of isoprenoids in the emissions of Norway spruce, four Scots pine chemotypes, and in boreal forest ambient air during HUMPPA-COPEC-2010. *Atmos. Chem. Phys.*, **12**, 7215–7229, doi:10.5194/acp-12-7215-2012.

Zhou, L., T. Nieminen, D. Mogensen, S. Smolander, A. Rusanen, M. Kulmala, and M. Boy, 2014: SOSAA—A new model to simulate the concentrations of organic vapours, sulphuric acid and aerosols inside the ABL—Part 2: Aerosol dynamics and one case study at a boreal forest site. *Boreal Environ. Res.*, **19**, 237–256.

Zieger, P., and Coauthors, 2015: Low hygroscopic scattering enhancement of boreal aerosol and the implications for a columnar optical closure study. *Atmos. Chem. Phys.*, **15**, 7247–7267, doi:10.5194/acp-15-7247-2015.